Supplementary Information (SI)

GENERAL-PURPOSE PASSIVE WIRELESS POINT-OF-CARE PLATFORM BASED ON SMARTPHONE

Pablo Escobedo*[1,3], Miguel M. Erenas*[2,3], Antonio Martínez-Olmos[1,3], Miguel A. Carvajal[1,3], Sara Gonzalez-Chocano[2], Luis Fermín Capitán-Vallvey[2,3], and Alberto J. Palma[1,3]

[1] ECsens, CITIC-UGR, Department of Electronics and Computer Technology, University of Granada, Campus Aynadamar, 18071 Granada, Spain.

[2] ECsens. Department of Analytical Chemistry. Campus Fuentenueva, Faculty of Sciences, 18071, University of Granada, Spain.

[3] Unit of Excellence in Chemistry applied to Biomedicine and the Environment of the University of Granada, Granada, Spain.

Corresponding author: Alberto J. Palma (ajpalma@ugr.es)

*Both authors have equally contributed to this work.

Table of Contents

Electrical characterization

Numerical simulations of the inductive coupling between the smartphone coil and our system antenna have been computed with COMSOL software. From this calculation, the magnetic flux density and flux lines are depicted in Figure S1(a) with a separation of 8 mm between both coils. This coupling is characterized by the mutual inductance, M, defined as the total magnetic flux intercepted by one antenna per unit of current flowing in the other antenna. Due to the coupling mechanism is dominated by near-field inductive effects, it was sufficient to compute the mutual inductance for the static case (frequency equals zero) and neglect capacitive effects along with wave propagation phenomena. The decrease of the inductive coupling with the antenna separation was also computed through the coupling constant, k, defined in Eq. S1 as

$$k = \frac{M}{\sqrt{L_1 \cdot L_2}} \qquad (Eq.\ S1)$$

where L_1 and L_2 are the inductance of the smartphone and our system coils respectively. In Figure S1(b), the normalized coupling constant, k/k_0, is depicted as a function of the coil separation, showing the decrease of the mutual inductance. k_0 is the maximum coupling constant between coils when aligned. Our experimental characterization pointed out 8.4 mm as the maximum separation before the platform turned off. Therefore, 93% maximum coupling is required to power up our system, resulting in an accurate antenna positioning. This set up was accomplished with the methacrylate-made holder accessory (see Figures 1(a) and 1(b) in the main text).

Potentiostat performance can be evaluated in the oscilloscope screenshots showed in Figures S1(c) and S1(d). In the first case, a triangular voltage waveform typically used in cyclic voltammetry is obtained, while in Figure S1(d), a bipolar pulse waveform, which can be used in ECL technique, is depicted demonstrating the versatility of the developed platform. Indeed, up to 25 different voltage levels from -1.15 to 1.15 V can be programmed with this potentiostat.
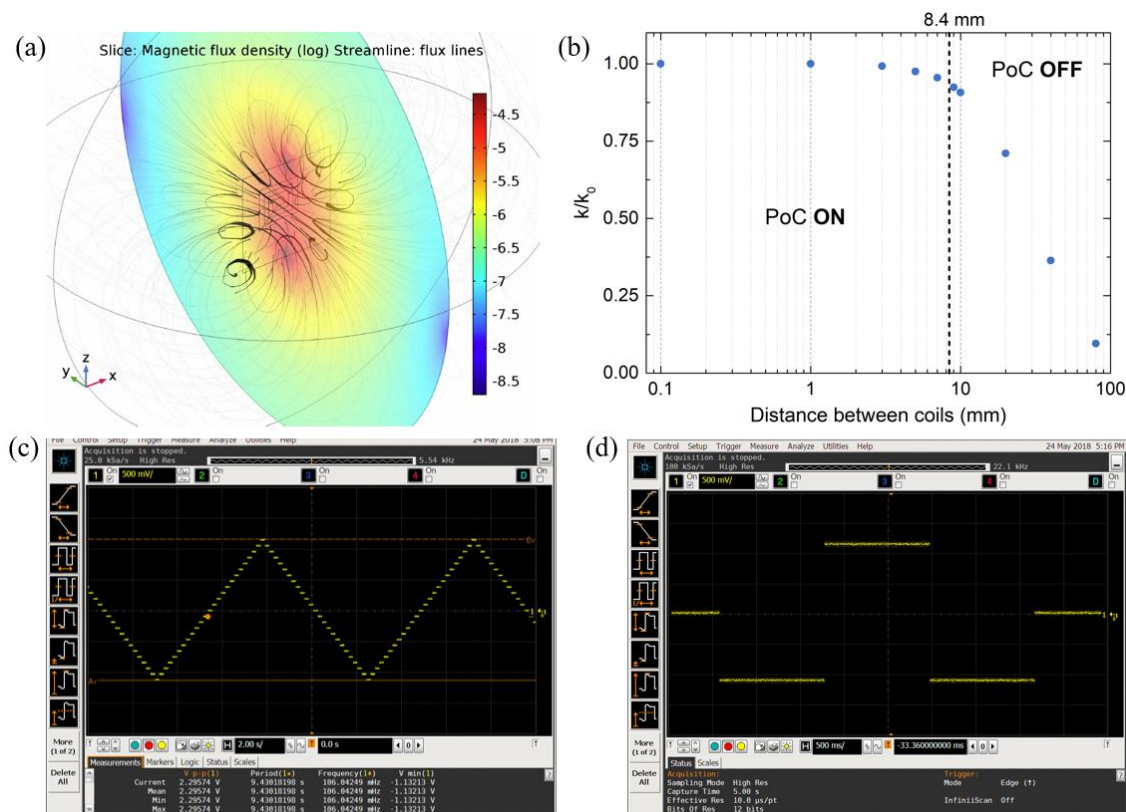
Figure S1. Electrical characterization. (a) Numerical simulation of the magnetic flux density (logarithmic scale) and flux lines. The contours of both antennas (smartphone reader and our system coil) are visible in the centre of the plot. (b) Normalized coupling factor as a function of the distance between coils, showing the separation intervals where PoC is ON or OFF. (c) Oscilloscope screenshot of the generated triangular waveform used in cyclic voltammetry. (d) Oscilloscope screenshot of a generated pulse waveform used for ECL.

Description of the Android™ application

The custom developed Android application provides several screens that guide the user through the different analytical procedures that can be conducted. The home-page of the application, shown in Figure S2(a), consists of a main menu that allows the user to choose among the four experimental methods: potentiometry, amperometry, voltammetry and ECL. When selecting each of the procedures, the application automatically sends to the PoC platform a specific command by means of the NFC interface so that the platform configures its programming accordingly to the selected method. For instance, if the user selects the amperometry technique, a new screen as the one in Figure S2(b) appears, which captures and displays the real-time data during the amperometry measurements. In the case of cyclic voltammetry, a configuration page is firstly showed to let the user specify the different parameters during the analytical procedure: initial and final voltages,

scan rate and number of cycles (see Figure S2(c)). After the configuration, the Start button will open a new screen (Figure S2(d)) where the real-time data is displayed during the cyclic voltammetry experiment according to the configured parameters. In the case of ECL, the last item of the main menu opens the screen of Figure S2(f), where the application takes control of the smartphone rear camera to perform the capture and subsequent processing of the ECL signal. All the data and graphs obtained in the smartphone during the different analytical procedures can be shared through email and different messaging services such as Facebook, Twitter and WhatsApp. To this end, the "Share" button has been enabled in the top menu of the application (see Figure S2(e)).
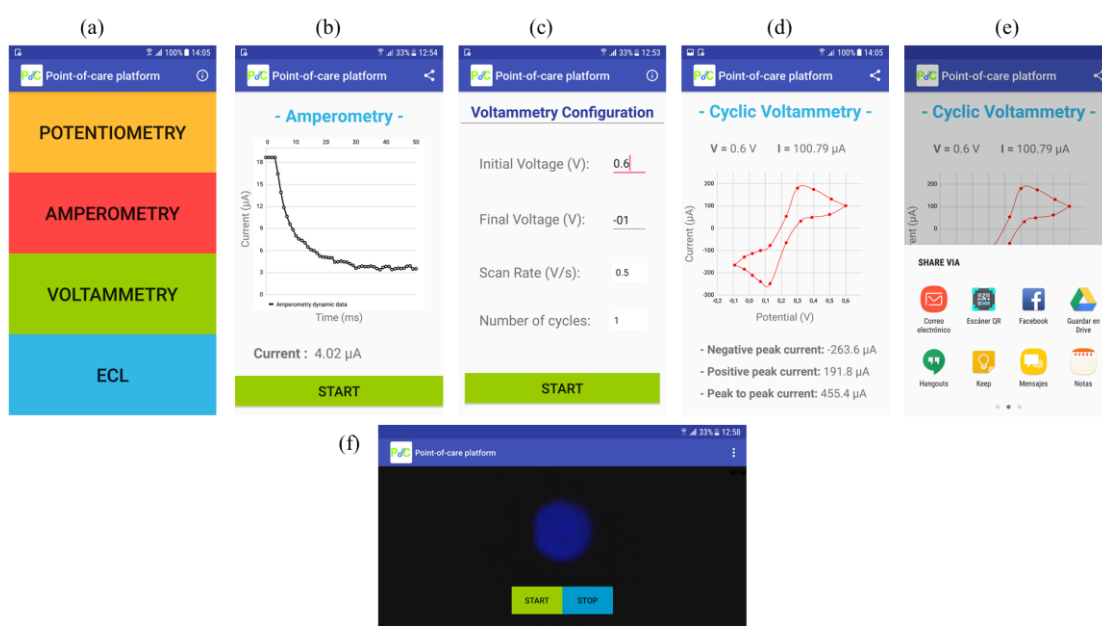

Figure S2. The custom-developed smartphone application for analytical procedure setting, optical and electrical signals processing, and display and sharing of results. (a) Home-page of the application for the election of the analytical procedure. (b) Real-time data display of amperometry during glucose calibration. (c) Configuration page of the different parameters for cyclic voltammetry operation. (d) Real-time data display of cyclic voltammetry. (e) Available data sharing and uploading options. (f) Screen capture of the application showing an optical ECL signal captured with the smartphone built-in rear video camera.

Cost study

A cost breakdown of the proposed platform is provided in Table S1. It can be seen that the total price of the system is around US$7.69 under mass production. This price is based on a wholesale order from two online electric component suppliers (Digi-Key Corporation and Mouser Electronics, Inc). It is expected that the cost of the PCB manufacturing would be only a small percentage of the total components cost under mass

production. The platform cost would increase up to US$15.91 in terms of components cost if just one unit is fabricated.

Table S1. List of prices (in US dollars) and sources for the components in the PoC platform.

Component	Supplier	Number of components required	Unit price (1 unit)	Unit price (wholesale)
AS3955	Mouser	1	$1.92	$0.683 (10000 units)
LMP91000	Mouser	1	$4.21	$2.03 (5000 units)
PIC16LF1703	Mouser	1	$0.87	$0.721 (100 units)
INA321	Mouser	1	$2.85	$1.26 (5000 units)
ADM660	Digi-Key	1	$4.64	$2.7866 (2500 units)
SMD resistor	Digi-Key	8	$0.10	$0.00127 (10000 units)
SMD ceramic capacitor	Digi-Key	2	$0.10	$0.0024 (15000 units)
SMD tantalum capacitor	Mouser	3	$0.14	$0.063 (8000 units)
Total		**18**	**$15.91**	**$7.685**

Device performance

Cyclic voltammetry:

The redox couple $[Fe(CN)_6^{3-}]/[Fe(CN)_6^{4-}]$ was used to test the cyclic voltammetry and potentiometry. Cyclic voltammetry was carried out by the addition to the SPE of 20 µL of $K_4[Fe(CN_6)]$ solution 3.4 mM in KCl 1 M. Then, potentials varying from -0.1 to 0.6 V were applied at a scan rate of 0.5 V/s, obtaining in this way the typical cyclic voltamperogram of $[Fe(CN)_6^{3-}]/[Fe(CN)_6^{4-}]$.

Potentiometry:

In the case of the potentiometry, solutions with different ratios $[Fe(CN)_6^{3-}]/[Fe(CN)_6^{4-}]$ were prepared and the potential difference was measured after 30 s. The potential depends on the ratio, and the ratios tested were 0.0, 0.3, 0.6, 0.9, 1.2, 1.5, 2.1 and 2.4. Both methods were performed using the reference instrument and our portable system, and the obtained results were then compared (Figure S3).
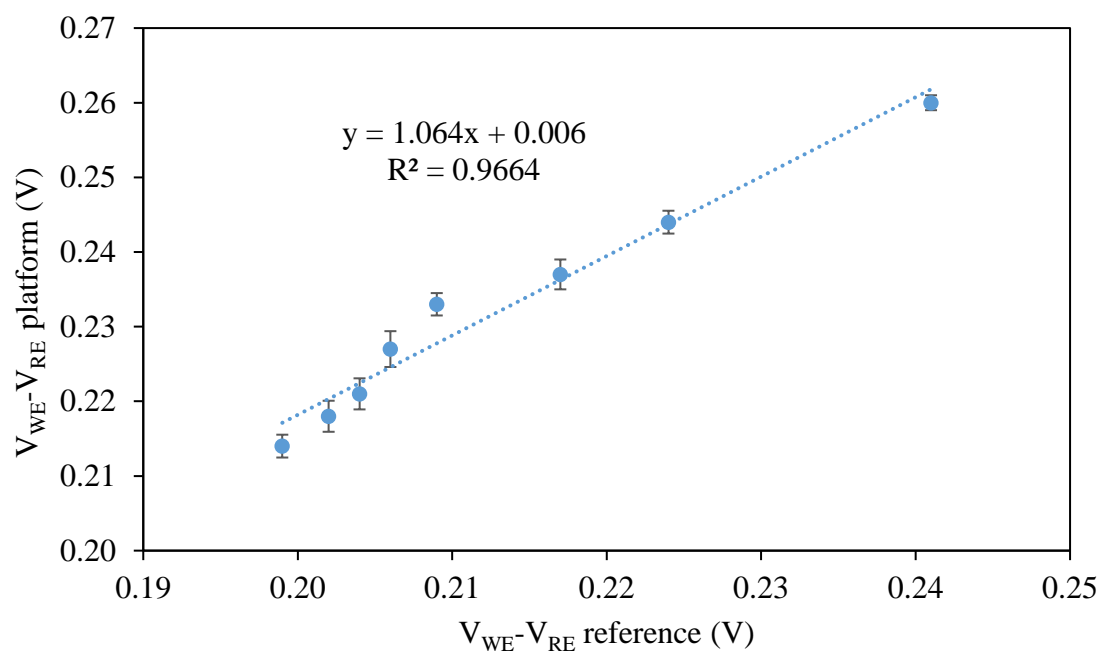
Figure S3. Correlation between potential obtained by the reference instrument and the developed platform for different $[Fe(CN)_6^{3-}]/[Fe(CN)_6^{4-}]$ ratios. V_{WE} -V_{RE} is the potential difference between the working and reference electrodes**.**

Electrochemiluminescence:

Luminol was selected to check the viability of performing ELC measurements using the smartphone along with the designed application. In this case, the ECL is generated by luminol when a potential of 0.5 V is applied in presence of H_2O_2. For this purpose, a 0.02 M solution of luminol in NaOH 0.1M and different H_2O_2 solutions in TRIS buffer 0.5M pH 9.0 were prepared, and 20 µL of each solution was added on a SPE to apply after that a 0.5 V pulse during 1 s. A number of H_2O_2 concentrations were tested to obtain the calibration (5.0, 8.0, 10.0, 20.0, 50.0 and 100.0 mM), measuring 5 replicates for each concentration. Analytical parameters were then obtained and compared for the reference instrument and our developed PoC platform. Figure S4 shows the correlation of the normalized optical intensities from the first applied voltage pulse obtained by both instruments, NOI_{MAX}.
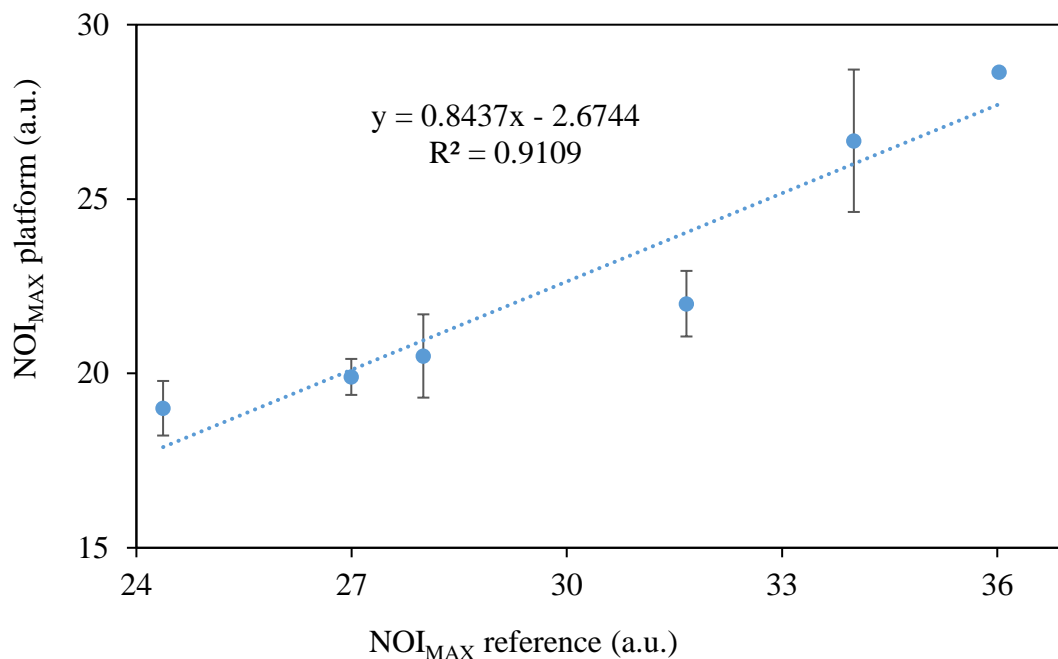
Figure S4. Correlation of the ECL normalized optical intensities (NOI$_{MAX}$) obtained by the reference instrument and the developed PoC.

Analytical procedures

Amperometric determination of glucose

Amperometric measurements of glucose (Nie et al., 2010) were performed by the addition on the screen-printed electrode (SPE) of 20 µL of glucose oxidase 250 U/mL solution in 1.0 M KCl, then 20 µL of K$_3$[Fe(CN)$_6$] 600 mM and, finally, 20 µL of a glucose standard. Afterwards, current intensity was measured after applying 0.6 V during 60 s. Calibration function was obtained by the assaying of 8 different glucose concentration solutions (0.750, 0.500, 0.250, 0.100, 0.075, 0.050, 0.025 y 0.010 M) in PBS buffer 0.1M and pH 7.0, obtaining eight replicates each. The glucose determination is done by oxidation of ferrocyanide on electrode. The generated quantity of ferrocyanide depends on the concentration of glucose in the sample, and the change of the generated current when 0.6 V is applied is related to the Fe(CN)$_6^{4-}$ produced during the reactions. Both the reference and our smartphone-based instruments were used to perform the measurements and to compare the results. Figure S5 shows the good correlation of the currents obtained.
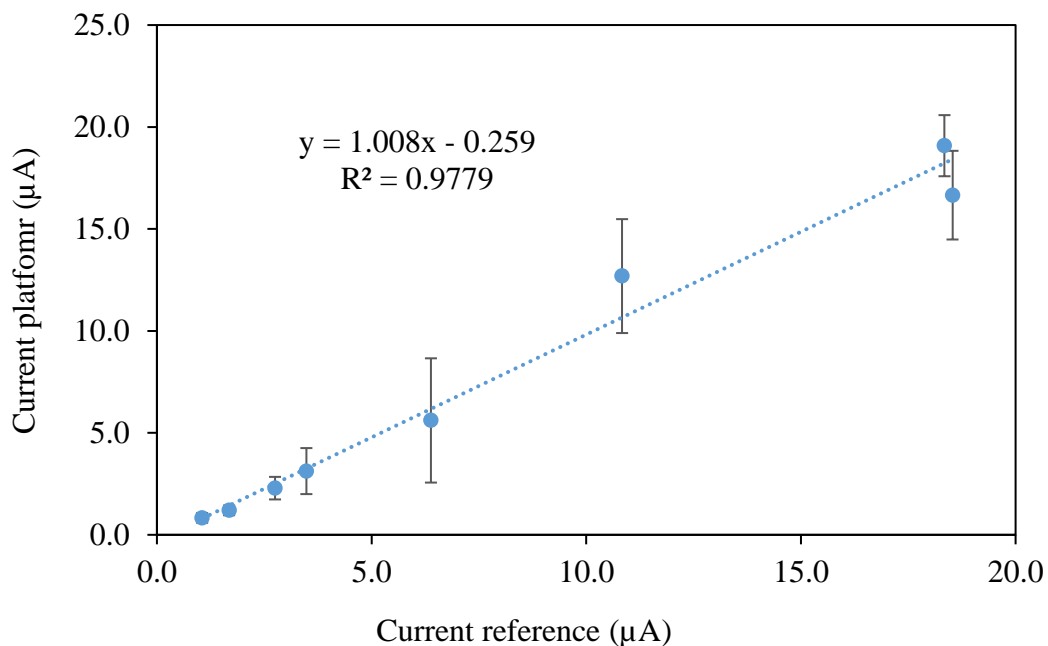
$$y = 1.008x - 0.259$$
$$R^2 = 0.9779$$

Figure S5. Correlation of the currents obtained by the reference instrument and the developed platform for amperometric glucose determination.

pH measurement

pH measurements are based on a polyaniline (PANI) coated working electrode, and the measurements of the potential difference between the working and reference electrodes at different pHs. Due to the transition of PANI from emeraldine salt to emeraldine base depending on the pH of the sample, the potential difference between the electrode changes. The coating of the working electrode with polyaniline (PANI) was performed by cyclic voltammetry. Firstly, the electrode was electrochemically cleaned by the addition of 60 µL of 0.5 M HCl, applying a potential from -0.3 V to 1.1 V at a scan rate of 0.1V/s for ten times. Then, 60 µL of aniline 0.1 M in 1.0 M HCl were added on the SPE and a potential from -0.2 to 1.0 V was applied at a scan rate of 0.1 V/S for ten times. Then the SPE was cleaned and 60 µL of 0.1M aniline were added again, and the previous process was repeated. When finished, the working electrode was coated with PANI film (Guinovart et al., 2014). Once the working electrode of the SPE was coated with PANI, the potential difference between the working and the reference electrode was measured after adding 40 µL of different pH solutions from 3 to 9. The potential difference was measured 30 s after the sample addition, which is the time needed to get a steady signal,

with three replicates per sample. The pH of the solutions tested was fixed by the use of phosphate buffer (PBS) 0.1 M. The potential differences were measured using both the reference instrument and our PoC system. Figure S6 shows the correlation of the potential difference obtained by the reference instrument and the developed platform.
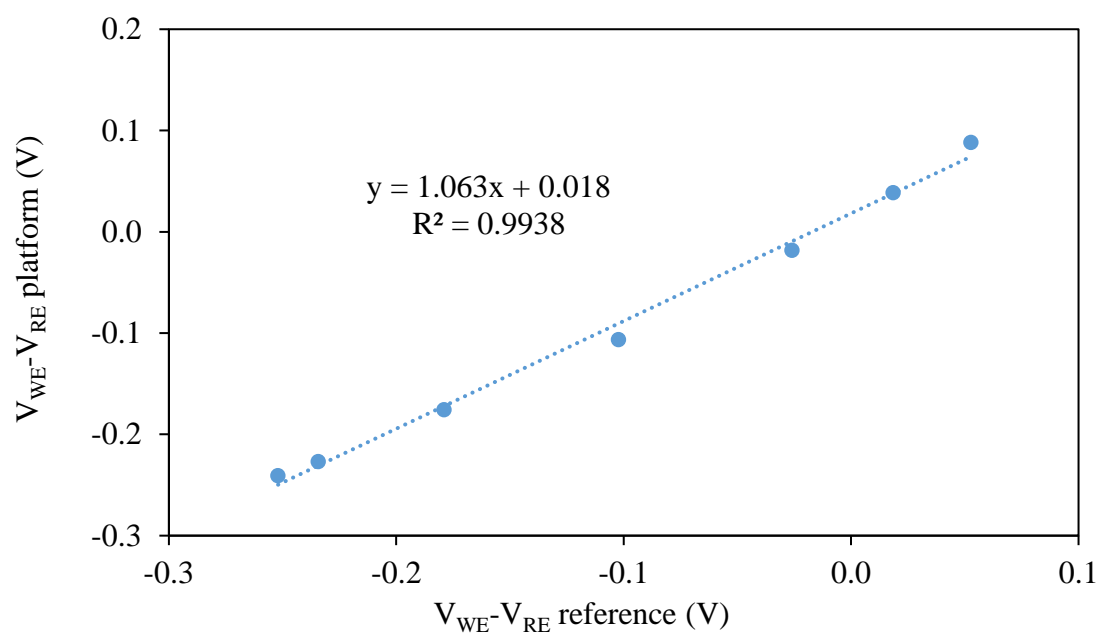

Figure S6. Correlation of the potential difference obtained by the reference instrument and our PoC system for the potentiometric determination. V_{WE} -V_{RE} is the potential difference between the working and reference electrodes. Error bars are included but with a length smaller than the dot diameter.

SI Bibliography

Guinovart, T., Valdés-Ramírez, G., Windmiller, J.R., Andrade, F.J., Wang, J., 2014. Bandage-Based Wearable Potentiometric Sensor for Monitoring Wound pH. Electroanalysis 26, 1345–1353. https://doi.org/10.1002/elan.201300558

Nie, Z., Nijhuis, C.A., Gong, J., Chen, X., Kumachev, A., Martinez, A.W., Narovlyansky, M., Whitesides, G.M., 2010. Electrochemical sensing in paper-based microfluidic devices. Lab Chip 10, 477–483. https://doi.org/10.1039/B917150A